

State Estimation with Model Reduction and Shape Variability. Application to biomedical problems.

Felipe Galarce, Damiano Lombardi, Olga Mula

June 18, 2021

Abstract

We develop a mathematical and numerical framework to solve state estimation problems for applications that present variations in the shape of the spatial domain. This situation arises typically in a biomedical context where inverse problems are posed on certain organs or portions of the body which inevitably involve morphological variations. If one wants to provide fast reconstruction methods, the algorithms must take into account the geometric variability. We develop and analyze a method which allows to take this variability into account without needing any a priori knowledge on a parametrization of the geometrical variations. For this, we rely on morphometric techniques involving Multidimensional Scaling, and couple them with reconstruction algorithms that make use of reduced model spaces pre-computed on a database of geometries. We prove the potential of the method on a synthetic test problem inspired from the reconstruction of blood flows and quantities of medical interest with Doppler ultrasound imaging.

1 Introduction

Model Order Reduction is nowadays an established class of methods to foster the application of mathematical modelling and scientific computing in realistic industrial contexts [1, 2]. Data Assimilation is an example of a field which is related to a broad spectrum of applications in science and engineering (the reader is referred to [3, 4]). Data Assimilation problems often come with a computational burden making them prohibitively hard to be solved. A classical way to formulate such problems reads as follows: a mathematical model formally links data and parameters of a system to its state (and, ultimately, the quantities of interest); given the measurements (which are partial and corrupted observations of the system state) we wish to estimate the state (what we refer to as state estimation) or the quantities of interest by repeatedly solving the model and improving its likelihood. In this work, we call the model Full Order Model (FOM), and the only fact that we need to evaluate it multiple times implies a large computational cost. To overcome this issue, we replace the evaluation of a costly FOM by a significantly less expensive Reduced-Order model (ROM), built by leveraging the properties of the sets of solutions of the FOM, as investigated for instance in [5, 6, 7, 8, 9].

One of the most common strategies to construct a ROM consists in dividing the procedure into two stages: in the *offline* stage, several instances of the FOM are solved, once and for all. The set of solutions makes it possible to uncover eventual sparse or low rank structures, to be exploited in the *online* phase, in which new instances are approximately solved by taking advantage of the knowledge acquired in the offline phase. The typical scenario in which this is applied is when the model is described by a parametric

Partial Differential Equation (PDE). The model variability is well described by a set of scalar parameters, which can be sampled in order to construct the solution set and the ROM.

Challenging scenarios are the ones in which the geometry of the domain can vary and it is potentially the unknown of the problem to be solved. This is common to several fields of research such as shape optimisation ([10, 11, 12]), inverse scattering problems ([13]), geometry morphometrics ([14, 15]). Moreover, a variable domain is challenging for projection based ROM for which, typically, a basis of space functions is defined on a given domain. This important issue has been studied in several works in the literature. A first example is provided in [16], in which a reduced-element method is devised, to take advantage of domain decomposition techniques and adapt to various potentially deformed domains. An important class of methods consists in mapping the domains into a same reference configuration and write the equations in this latter. In [17] the authors consider the set of transformations with affine parametrisation and their effect on the inf-sup stability for a reduced-basis formulation of the Stokes problem. In [18], the computational domain is deformed thanks to an elastic displacement and the non-affine dependence of the equations on the domain is tackled by using a matrix-DEIM approach. A similar approach is proposed in [19] to efficiently reduce the computational cost of parametrised fluid models. In [20] an isogeometric analysis framework is used to deal with the domain parametrisation and build a reduced-basis method to speed up shape optimisation problems. A similar approach is proposed in [21]. In [22] the parametrisation of the domain (obtained by considering NURBS) is incorporated as extra-coordinate in a Progressive Generalised Decomposition (PGD) method. In [23] a free-form deformation method is coupled to Proper Orthogonal Decomposition (POD) in the context of shape optimisation in aerodynamics. In [24], instead of mapping the domains into a common reference configuration, the shifted boundary method is applied to deal with the geometry parametrisation. By doing so, we avoid the changes of coordinate; to deal with the intrinsic non-linearity, the authors propose to use the GNAT method or the gappy-POD. In [25] an hyper-reduction framework is used to deal with non-parametrised geometrical variations of the domain in the context of fluid-mechanics. In [26] a reduced-basis formulation is proposed to deal with a cut-FEM embedding method. In [27] the reduced-basis functions are defined on an average-deformed configuration in order to speed up finite volume computations for fluid models with variable geometries. In [28] the authors consider the problem of the parametrisation of interfaces in the context of fluid-structure interaction problems. In [29], the reduced-basis method is used to efficiently solve the Maxwell equations to speed up the design of semiconductors. In [30, 31] and other recent works, the authors consider the problem of registration applied to model reduction: by suitably transforming the domain we can achieve the reduction efficiency. Numerous applications including geometry reduction can take advantage of such techniques.

The present work was motivated by applications in biomedical engineering. The prototypical yet fundamental situation regards the clinical applications in which non-invasive measurements (typically acquired by medical imaging) are exploited in order to infer non-observable mechanical or physiological properties, or to perform state estimation. The time constraints of the clinical applications clearly motivate and justify the use of ROMs. However, the inter-patient variability is often very large and manifests itself also in terms of anatomy, hence domain geometry. This points towards a severe limitation of the classical ROM strategy, as typically one would need to construct a database of FOM solutions for each patient, reducing the range of possible applications to the ones in which we monitor a patient multiple times and follow the pathology evolution.

With respect to the works cited above, there are two major differences. First, we set up a reduced-order method specifically tailored for the task of the *inverse* data-assimilation problem with shape variability. This is in contrast with the above works, which focus mostly on the *direct* problem but we emphasize that our method is general and it could be adapted for that purpose. Second, our proposed strategy is nonparametric in the sense that it does not require any a priori knowledge on an explicit

parametrization of the geometry, and it does not require to define a reference geometry.

To the best of our knowledge, the work which shares more similarities with the present contribution is [32]. In that work, a set of realistic patient template geometries is built without knowing the underlying, potentially high-dimensional, parametrisation. The authors then construct the reduced-order model on a geometry computed as the average of the available templates. A set of transformations make it possible to map fields between the geometries and the average geometry. The two main differences with respect to the present work are the following: we construct a reduced-order method in view of performing the reconstruction given some observable so, instead of constructing an atlas based solely on geometric information, we construct a set of templates based also on the physics of the problem we are considering. In order to solve the Data Assimilation problem in a reduced way, we adapt the Parametrised Background Data Weak approach, proposed in [33] and analyzed in subsequent papers such as [34, 35, 36, 37, 38, 39, 40].

The structure of the work is as follows: in Section 2 we present the context of the state estimation and the methods we use in the present work. In 3 we detail the strategy we adopt in order to deal with variable domain geometries. In 4 we propose an error analysis for the Data Assimilation problem. In section 5 we describe in detail how the different steps of the procedure are practically implemented and we conclude by presenting a numerical experiment to assess the method.

2 Multi-Domain State Estimation: Problem Setting

In the following, the terms geometry, spatial domain, and shape will be used interchangeably whenever there is not ambiguity.

2.1 State estimation on a given domain

Let Ω be a fixed given domain of \mathbb{R}^d with dimension $d \geq 1$, and let $V(\Omega)$ be a Hilbert space defined over Ω . The space is endowed with an inner product $\langle \cdot, \cdot \rangle$ and induced norm $\| \cdot \|$. The choice of $V(\Omega)$ must be relevant for the problem under consideration, and typical options are L^2 , H^1 or some Reproducing Kernel Hilbert Space.

Our goal is to recover an unknown function $u \in V(\Omega)$ from m possibly noisy measurement observations

$$y_i = \ell_i(u) + \eta_i, \quad i = 1, \dots, m,$$

where the ℓ_i are linearly independent linear forms from $V'(\Omega)$ and the η_i are unknown measurement errors. In the following, for the sake of simplicity, we will assume that there is no noise ($\eta_i = 0$, $i = 1, \dots, m$) but the main methodology which we develop could easily be extended to deal with noisy measurements. In practical applications, each ℓ_i models a sensor device which is used to collect the measurement data $\ell_i(u)$. In the applications which we present in our numerical tests, the observations come in the form of an image and each ℓ_i models the response of the system on a given pixel as Figure 4 illustrates.

We denote by $\omega_i \in V(\Omega)$ the Riesz representers of the ℓ_i . They are defined via the variational equation

$$\langle \omega_i, v \rangle = \ell_i(v), \quad \forall v \in V(\Omega).$$

Since the ℓ_i are linearly independent in $V'(\Omega)$, so are the ω_i in $V(\Omega)$ and they span an m -dimensional space

$$W_m(\Omega) = \text{span}\{\omega_1, \dots, \omega_m\} \subset V(\Omega)$$

When there is no measurement noise, knowing the observations $y_i = \ell_i(u)$ is equivalent to knowing the orthogonal projection

$$\omega = P_{W_m(\Omega)} u.$$

In this setting, the task of recovering u from the measurement observation ω can be viewed as building a recovery algorithm

$$A : W_m(\Omega) \mapsto V(\Omega)$$

such that $A(P_{W_m(\Omega)}u)$ is a good approximation of u in the sense that $\|u - A(P_{W_m(\Omega)}u)\|$ is small.

Recovering u from the measurements $P_{W_m(\Omega)}u$ is a very ill-posed problem since $V(\Omega)$ is generally a space of very high or infinite dimension so, in general, there are infinitely many $v \in V(\Omega)$ such that $P_{W_m(\Omega)}v = \omega$. It is thus necessary to add some a priori information on u in order to recover the state up to a guaranteed accuracy. In the following, we work in the setting where u is a solution to some parameter-dependent PDE of the general form

$$\mathcal{P}(u, y) = 0,$$

where \mathcal{P} is a differential operator and y is a vector of parameters that describes some physical property and lives in a given set $Y \subset \mathbb{R}^p$. For every $y \in Y$, we assume that the PDE has a unique solution $u = u(y) \in V(\Omega)$. Therefore, our prior on u is that it belongs to the set

$$\mathcal{M}(\Omega) := \{u(y) \in V(\Omega) : y \in Y\},$$

which is sometimes referred to as the *solution manifold*.

Performance Benchmarks: The quality of a recovery mapping A is usually quantified in two ways:

- If the sole prior information is that u belongs to the manifold $\mathcal{M}(\Omega)$, the performance is usually measured by the worst case reconstruction error

$$E_{\text{wc}}(A, \mathcal{M}(\Omega)) = \sup_{u \in \mathcal{M}(\Omega)} \|u - A(P_{W_m(\Omega)}u)\|.$$

- In some cases u is described by a probability distribution p on $V(\Omega)$ supported on $\mathcal{M}(\Omega)$. This distribution is itself induced by a probability distribution on Y that is assumed to be known. When no information about the distribution is available, usually the uniform distribution is taken. In this Bayesian-type setting, the performance is usually measured in an average sense through the mean-square error

$$E_{\text{ms}}^2(A, \mathcal{M}(\Omega)) = \mathbb{E}(\|u - A(P_{W_m(\Omega)}u)\|^2) = \int_{V(\Omega)} \|u - A(P_{W_m(\Omega)}u)\|^2 dp(u),$$

and it naturally follows that $E_{\text{ms}}(A, \mathcal{M}(\Omega)) \leq E_{\text{wc}}(A, \mathcal{M}(\Omega))$.

PBDW as our practical algorithm: In this work, we will reconstruct with the Parametrized-Background Data-Weak algorithm (PBDW, [33]). Other choices would of course be possible but the PBDW algorithm is relevant for the following reasons:

- **Simplicity and Speed:** It is easily implementable and it provides reconstructions in near-real time.
- **Optimality:** It has strong connections with optimal linear reconstruction algorithms as has been studied in [35, 39].
- **Extensions:** If required, the algorithm can easily be extended to enhance its reconstruction performance (see [40, 41]). In particular, it shown in [40] that piece-wise PBDW reconstruction strategy can deliver near-optimal reconstruction performance. The PBDW algorithm can also be easily adapted to accommodate noisy measurements (see [36, 38]) and some easy-to implement extension to mitigate the model error exist (in the following however, we assume the PDE model is perfect for the sake of simplicity).

Since the geometry of $\mathcal{M}(\Omega)$ is generally complex, optimization tasks posed on $\mathcal{M}(\Omega)$ are difficult (lack of convexity, high evaluation costs for different parameters). Therefore, instead of working with $\mathcal{M}(\Omega)$, PBDW works with a linear (or affine) space $V_n(\Omega)$ of reduced dimension n which is expected to approximate the solution manifold well in the sense that the approximation error of the manifold

$$\delta_n^{(\text{wc})} := \sup_{u \in \mathcal{M}(\Omega)} \text{dist}(u, V_n(\Omega)), \quad \text{or} \quad \delta_n^{(\text{ms})} := \mathbb{E} \left(\text{dist}(u, V_n(\Omega))^2 \right)^{1/2}$$

decays rapidly if we increase the dimension n . It has been proven in [42] that it is possible to find such hierarchies of spaces $(V_n(\Omega))_{n \geq 1}$ for certain manifolds coming from classes of elliptic and parabolic problems, and numerous strategies have been proposed to build the spaces in practice (see, e.g., [43, 44] for reduced basis techniques and [42, 45] for polynomial approximations in the y variable).

Assuming that we are given a reduced model $V_n(\Omega)$ with $1 \leq n \leq m$, the PBDW algorithm

$$A_{m,n}^{(\text{pbdw})} : W_m \rightarrow V(\Omega)$$

gives for any $\omega \in W_m(\Omega)$ a solution of

$$A_{m,n}^{(\text{pbdw})}(\omega) \in \arg \min_{u \in \omega + W(\Omega)^\perp} \text{dist}(u, V_n(\Omega)). \quad (2.1)$$

The minimizer is unique as soon as $n \leq m$ and $\beta(V_n(\Omega), W_m(\Omega)) > 0$, which is an assumption to which we adhere in the following. In practice, solving problem (2.1) boils down to solving a linear least squares minimization problem. We refer, e.g., to [46, Appendix A] for details on how to compute it in practice. For any pair of closed subspaces (E, F) of V , $\beta(E, F)$ is defined as

$$\beta(E, F) := \inf_{e \in E} \sup_{f \in F} \frac{\langle e, f \rangle}{\|e\| \|f\|} = \inf_{e \in E} \frac{\|P_F e\|}{\|e\|} \in [0, 1].$$

We can prove that $A_{m,n}^{(\text{pbdw})}$ is a bounded linear map from $W_m(\Omega)$ to $V_n(\Omega) \oplus (W_m(\Omega) \cap V_n(\Omega)^\perp)$. In fact, it is a simple least squares problem whose cost is essentially n^2 . Therefore, if the dimension n of the reduced model is moderate, the reconstruction with (2.1) takes place in close to real-time.

For any $u \in V(\Omega)$, the reconstruction error is bounded by

$$\|u - A_{m,n}^{(\text{pbdw})}(\omega)\| \leq \beta^{-1}(V_n, W_m) \|u - P_{V_n \oplus (W_m \cap V_n^\perp)} u\| \leq \beta^{-1}(V_n, W_m) \|u - P_{V_n} u\|, \quad (2.2)$$

where we have omitted the dependency of the spaces on Ω in order not to overload the notation, and we will keep omitting this dependency until the end of this section. Depending on whether V_n is built to address the worst case or mean square error, the reconstruction performance over the whole manifold \mathcal{M} is bounded by

$$e_{m,n}^{(\text{wc}, \text{pbdw})} := E_{\text{wc}}(A_{m,n}^{(\text{pbdw})}, \mathcal{M}) \leq \beta^{-1}(V_n, W_m) \max_{u \in \mathcal{M}} \text{dist}(u, V_n \oplus (V_n^\perp \cap W_m)) \leq \beta^{-1}(V_n, W_m) \delta_n^{(\text{wc})},$$

or

$$\begin{aligned} e_{m,n}^{(\text{ms}, \text{pbdw})} &:= E_{\text{ms}}(A_{m,n}^{(\text{pbdw})}, \mathcal{M}) \leq \beta^{-1}(V_n, W_m) \mathbb{E} \left(\text{dist}(u, V_n \oplus (V_n^\perp \cap W_m))^2 \right)^{1/2} \\ &\leq \beta^{-1}(V_n, W_m) \delta_n^{(\text{ms})}. \end{aligned} \quad (2.3)$$

Note that $\beta(V_n, W_m)$ can be understood as a stability constant. It can also be interpreted as the cosine of the angle between V_n and W_m . The error bounds involve the distance of u to the space $V_n \oplus (V_n^\perp \cap W_m)$ which provides slightly more accuracy than the reduced model V_n alone. This term is the reason why it is sometimes said that the method can correct model error to some extent. In the following, to ease the reading we will write errors only with the second type of bounds (2.3) that do not involve the correction part on $V_n^\perp \cap W_m$.

An important observation is that for a fixed measurement space W_m (which is the setting in our numerical tests), the error functions

$$n \mapsto e_{m,n}^{(\text{wc}, \text{pbdw})}, \quad \text{and} \quad n \mapsto e_{m,n}^{(\text{ms}, \text{pbdw})}$$

reach a minimal value for a certain dimension n_{wc}^* and n_{ms}^* as the dimension n varies from 1 to m . This behavior is due to the trade-off between:

- the improvement of the approximation properties of V_n as n grows ($\delta_n^{(\text{wc})}$ and $\delta_n^{(\text{ms})} \rightarrow 0$ as n grows)
- the degradation of the stability of the algorithm, given here by the decrease of $\beta(V_n, W_m)$ to 0 as $n \rightarrow m$. When $n > m$, $\beta(V_n, W_m) = 0$.

As a result, the best reconstruction performance with PBDW is given by

$$e_{m, n_{\text{wc}}^*}^{(\text{wc}, \text{pbdw})} = \min_{1 \leq n \leq m} e_{m,n}^{(\text{wc}, \text{pbdw})}, \quad \text{or} \quad e_{m, n_{\text{ms}}^*}^{(\text{ms}, \text{pbdw})} = \min_{1 \leq n \leq m} e_{m,n}^{(\text{ms}, \text{pbdw})}.$$

2.2 Obstructions when the spatial domain is not given a priori

The speed of the above reconstruction algorithm crucially relies on the fact that we have assumed that the spatial domain Ω is given to us a priori. Thanks to this we can precompute the reduced models $V_n(\Omega)$ before the reconstruction takes place, and we only need to solve (2.1) during the reconstruction, which is a computation that can be done in near real-time. The offline computation of the reduced model should be seen as a training phase, and it can be computationally intensive and time-consuming for complex physical systems.

There are however cases in which we cannot assume that Ω is given a priori. This situation typically arises in biomedical applications where state estimation needs to be performed on a certain part of the body for different patients which inevitably present morphological variations. In this case, given a new target geometry Ω , one could of course generate $\mathcal{M}(\Omega)$ and derive a reduced model $V_n(\Omega)$ but this task would not be feasible in real-time, and the method would not be useful for real time decisions. To avoid this computational bottleneck, we propose a method to quickly build a space $V_n(\Omega)$ by using reduced models which have been pre-computed on a database of template geometries which we suppose to be available offline. The idea consists in finding the best reduced model from the template geometries, and then to transport it to the target geometry Ω . Once this is done, we reconstruct with PBDW on the target geometry. The next section presents the details of our proposed strategy.

3 Proposed strategy for fast state estimation

We consider a set G of spatial domains in \mathbb{R}^d . The set can potentially be infinite. An example for G is the set of human carotid arteries or, more generally, the set of shapes of a certain organ. Our goal is to build a state estimation procedure that is fast for every geometry $\Omega \in G$. For this, our approach is based on a learning phase that involves computations on a dataset of available template geometries. We next summarize the main steps. In section 4 we give an error analysis of the procedure and discuss the main sources of inaccuracy. Some steps involve certain routines which are introduced at an abstract level in this section and in the error analysis. In section 5, we explain how we have implemented them in practice, and how our theory justifies certain choices. Note however that since the procedure is general, other constructions can of course be considered for these building blocks.

Training/Learning phase (offline)

- **Database of Template Geometries:** Gather a family of K template domains

$$G_{\text{templates}} = \{\Omega_1, \dots, \Omega_K\} \subseteq G.$$

This family will serve as a database for our subsequent developments.

- **Database of Template Reduced Models:** For every $\Omega \in G_{\text{templates}}$, similarly as in section 2.1 we consider a parameter-dependent PDE

$$\mathcal{P}(u, y) = 0,$$

where the parameters y take values in Y and the solution $u(y)$ belongs to a Hilbert space $V(\Omega)$. Note that the differential operator \mathcal{P} and the parameter domain Y could vary with the geometry Ω . However, to simplify the presentation, we assume that \mathcal{P} and Y are taken identical for all $\Omega \in G_{\text{templates}}$. The set of solutions yields the solution manifold $\mathcal{M}(\Omega)$ and it describes all the possible physical states of the system under consideration for the given geometry. We summarize the physics by precomputing a template reduced model $V_n(\Omega)$,

$$\mathcal{M}(\Omega) \approx V_n(\Omega), \quad \forall \Omega \in G_{\text{templates}}.$$

- **Transport snapshots and reduced-models between geometries:** We need to define a map to transport function between different geometries

$$\tau_{\Omega \rightarrow \Omega'} : V(\Omega) \rightarrow V(\Omega'), \quad \forall (\Omega, \Omega') \in G \times G.$$

We also need to define a map to transport subspaces into subspaces. Since in general the image of a subspace $V_n(\Omega)$ by $\tau_{\Omega \rightarrow \Omega'}$ is not necessarily a subspace, we introduce another mapping

$$\hat{\tau}_{\Omega \rightarrow \Omega'} : V_n(\Omega) \subseteq V(\Omega) \rightarrow V_{n'}(\Omega') \subseteq V(\Omega'), \quad \forall (\Omega, \Omega') \in G \times G.$$

We assume in the following that $n' \leq n$. Also, for some applications, it will be important that τ satisfies some physical properties such as mass conservation. We discuss how we have built τ and $\hat{\tau}$ in practice in section 5.1.

- **Best-Template:** For the reconstruction task, we need to identify for each new target geometry $\Omega \in G$ which template geometry $\Omega_t \in G_{\text{templates}}$ has the most appropriate reduced model $V_n(\Omega_t)$ that we have to transport to Ω . For this, we need to build a best template map

$$\begin{aligned} \text{BT} : G &\rightarrow G_{\text{templates}} \\ \Omega &\mapsto \Omega_t^*. \end{aligned}$$

We discuss the different possibilities to build BT in section 5.2.

Reconstruction phase (online)

We are given a target domain $\Omega \in G$, and our goal is to give a fast reconstruction of an unknown function $u \in V(\Omega)$ given m measurement observations $\ell(u) = (\ell_i(u))_{i=1}^m$. Note that since $\ell_i \in V'(\Omega)$, the observation space depends on the geometry and $W = W(\Omega)$.

- If $\Omega \in G_{\text{templates}}$ (the target geometry is in our template dataset), then we simply reconstruct with $A_{n,m}^{(\text{pbdw})}(P_{W(\Omega)}u)$ with the pre-computed reduced model $V_n(\Omega)$.

- If $\Omega \notin G_{\text{templates}}$:
 - We need to find an appropriate reduced model for the reconstruction. For this, we apply the best-template mapping BT and we set

$$\Omega_t^* = \text{BT}(\Omega) \in G_{\text{templates}}.$$

- We transport the template reduced model $V_n(\Omega_t^*)$ to Ω by applying $\widehat{\tau}_{\Omega_t^* \rightarrow \Omega}$, namely

$$\widehat{V}_n(\Omega) = \widehat{\tau}_{\Omega_t^* \rightarrow \Omega}(V_n(\Omega_t^*))$$

- In Ω , we reconstruct with PBDW using $W_m(\Omega)$ and $\widehat{V}_n(\Omega)$.

4 Theoretical analysis of the reconstruction error

Suppose we are given a target geometry $\Omega_1 \in G$ and that we want to reconstruct an unknown function $u \in \mathcal{M}(\Omega_1)$ from its observations $\ell_i(u)$, $i = 1, \dots, m$. Suppose further that we fix a geometry $\Omega_0 \in G_{\text{templates}}$ and we transport the reduced model space $V_n(\Omega_0)$ to the target geometry by applying $\widehat{\tau}_{\Omega_0 \rightarrow \Omega_1}(V(\Omega_0))$. The goal of this section is to give an error bound on the reconstruction of $u \in \mathcal{M}(\Omega_1)$ with PBDW and using

$$\widehat{V}_n(\Omega_1) = \widehat{\tau}_{\Omega_0 \rightarrow \Omega_1}(V_n(\Omega_0))$$

as a reduced model on Ω_1 .

The results involve the following notion of Hausdorff distance between compact sets.

Definition 1. For any two given compact sets X and Y of a Hilbert space V , the Hausdorff distance between X and Y is defined as

$$d_H(X, Y) := \max\{\sup_{x \in X} \|x - P_Y x\|_V, \sup_{y \in Y} \|y - P_X y\|_V\}.$$

4.1 An error bound based on $d_H(\tau_{\Omega_0 \rightarrow \Omega_1} \mathcal{M}(\Omega_0), \mathcal{M}(\Omega_1))$

It is natural to expect that the reconstruction error will be of good quality if:

- the physical phenomena contained in the target manifold $\mathcal{M}(\Omega_1)$ are well represented in some sense by the transported manifold $\tau_{\Omega_0 \rightarrow \Omega_1} \mathcal{M}(\Omega_0)$, and if
- the reduced model $V_n(\Omega_0)$ approximates \mathcal{M}_0 with enough accuracy, and its quality is not degraded by the transport to the target geometry.

Theorem 4.1 formalises and quantifies this intuition under the following assumptions:

1. In the template geometry Ω_0 , the accuracy of the template reduced model $V_n(\Omega_0)$ is bounded by

$$\max_{u \in \mathcal{M}(\Omega_0)} \|u - P_{V_n(\Omega)} u\| \leq \varepsilon_0 \tag{H1}$$

for some $\varepsilon_0 \geq 0$.

2. The Hausdorff distance between $\tau_{\Omega_0 \rightarrow \Omega_1}(\mathcal{M}(\Omega_0))$ and $\mathcal{M}(\Omega_1)$ is bounded by

$$d_H(\tau_{\Omega_0 \rightarrow \Omega_1} \mathcal{M}(\Omega_0), \mathcal{M}(\Omega_1)) \leq \eta, \tag{H2}$$

for some $\eta \geq 0$. Note that $d_H(\tau_{\Omega_0 \rightarrow \Omega_1} \mathcal{M}(\Omega_0), \mathcal{M}(\Omega_1))$ couples the physics, the geometry and the transport between Ω_0 and Ω_1 . The bound on this term expresses the fact that the physics in the

target domain Ω_1 , expressed via the manifold $\mathcal{M}(\Omega_1)$, should be well represented when we transport the physics from Ω_0 to Ω_1 . The value of η could of course be large depending on the type of physics, geometries, and transport.

3. We finally need two technical assumptions on the transport maps $\tau_{0 \rightarrow 1}$ and $\widehat{\tau}_{0 \rightarrow 1}$:

(a) $\tau_{0 \rightarrow 1} : V(\Omega_0) \rightarrow V(\Omega_1)$ is Hölder continuous, namely there exists $C > 0$ and $\alpha > 0$ such that

$$\|\tau_{0 \rightarrow 1}(f) - \tau_{0 \rightarrow 1}(g)\|_{V(\Omega_1)} \leq C \|f - g\|_{V(\Omega_0)}^\alpha, \quad \forall (f, g) \in V(\Omega_0) \times V(\Omega_0). \quad (\text{H3})$$

(b) There exists $\gamma \geq 0$ such that

$$\sup_{v \in \tau_{0 \rightarrow 1}(V_n(\Omega_0))} \frac{\|v - P_{\widehat{\tau}_{0 \rightarrow 1}(V(\Omega_0))} v\|_{V(\Omega_1)}}{\|v\|_{V(\Omega_1)}} \leq \gamma. \quad (\text{H4})$$

Theorem 4.1. *Let $\Omega_0 \in \mathbf{G}_{templates}$ be a template geometry and let $u \in \mathcal{M}(\Omega_1)$ be a target function to estimate from the observations $P_{W_m(\Omega_1)} u$. If we reconstruct with PBDW using*

$$\widehat{V}_n(\Omega_1) = \widehat{\tau}_{0 \rightarrow 1}(V_n(\Omega_0))$$

then the reconstruction error is bounded by

$$\|u - A(P_{W_m(\Omega_1)} u)\|_{V(\Omega_1)} \leq \frac{1}{\beta(\widehat{V}_n(\Omega_1), W_m(\Omega_1))} \|u - P_{\widehat{V}_n(\Omega_1)} u\|_{V(\Omega_1)}. \quad (4.1)$$

If the assumptions (H1) to (H4) hold, then the reconstruction error over the whole manifold $\mathcal{M}(\Omega_1)$ is bounded by

$$\max_{u \in \mathcal{M}(\Omega_1)} \|u - A(P_W u)\|_{V(\Omega_1)} \leq \frac{1}{\beta(\widehat{V}_n(\Omega_1), W_m(\Omega_1))} (\eta + \max_{v \in \tau_{0 \rightarrow 1} \mathcal{M}(\Omega_0)} \|v - P_{\widehat{V}_n(\Omega_1)}(v)\|_{V(\Omega_1)}). \quad (4.2)$$

Suboptimal bounds for $\max_{v \in \tau_{0 \rightarrow 1} \mathcal{M}(\Omega_0)} \|v - P_{\widehat{V}_n(\Omega_1)}(v)\|_{V(\Omega_1)}$ are

$$\max_{v \in \tau_{0 \rightarrow 1} \mathcal{M}(\Omega_0)} \|v - P_{\widehat{V}_n(\Omega_1)}(v)\|_{V(\Omega_1)} \leq C \varepsilon_0^\alpha + \max_{v \in \tau_{0 \rightarrow 1} P_{V_n(\Omega_0)} \mathcal{M}(\Omega_0)} \|v - P_{\widehat{V}_n(\Omega_1)} v\|_{V(\Omega_1)} \quad (4.3)$$

$$\leq C(\varepsilon_0^\alpha + \gamma \max_{u \in \mathcal{M}(\Omega_0)} \|u\|_{V(\Omega_0)}^\alpha), \quad (4.4)$$

where the constant $C > 0$ is the one given in assumption (H3).

Proof. In this proof, all norms will be related to the space $V(\Omega_1)$ defined on the target geometry Ω_1 . Let $u \in \mathcal{M}(\Omega_1)$. By (2.2), we have

$$\|u - A(P_W u)\| \leq \frac{1}{\beta(\widehat{V}_n(\Omega_1), W)} \|u - P_{\widehat{V}_n(\Omega_1)} u\|, \quad (4.5)$$

which is the first inequality of the Theorem. We next bound $\|u - P_{\widehat{V}_n(\Omega_1)} u\|$ in terms of quantities in the template geometry Ω_0 and the transport operators $\tau_{0 \rightarrow 1}$ and $\widehat{\tau}_{0 \rightarrow 1}$. For this, let

$$u_1 \in \arg \inf_{v \in \tau_{0 \rightarrow 1}(\mathcal{M}(\Omega_0))} \|u - v\|,$$

and remark that

$$\|u - u_1\| \leq d_H(\tau_{0 \rightarrow 1}(\mathcal{M}(\Omega_0)), \mathcal{M}(\Omega_1)) \leq \eta \quad (4.6)$$

by assumption (H2).

By the triangle inequality and inequality (4.6),

$$\begin{aligned} \|u - P_{\widehat{V}_n(\Omega_1)} u\| &\leq \|u - u_1 - P_{\widehat{V}_n(\Omega_1)}(u - u_1)\| + \|u_1 - P_{\widehat{V}_n(\Omega_1)} u_1\| \\ &\leq \eta + \|u_1 - P_{\widehat{V}_n(\Omega_1)} u_1\| \\ &\leq \eta + \max_{v \in \tau_{0 \rightarrow 1} \mathcal{M}(\Omega_0)} \|v - P_{\widehat{V}_n(\Omega_1)} v\|, \end{aligned} \quad (4.7)$$

and the error bound (4.2) follows by inserting (4.7) into (4.5).

We next bound $\max_{v \in \tau_{0 \rightarrow 1} \mathcal{M}(\Omega_0)} \|v - P_{\widehat{V}_n(\Omega_1)} v\|$ as follows. For any $u_1 \in \tau_{0 \rightarrow 1} \mathcal{M}(\Omega_0)$, there exists $u_0 \in \mathcal{M}(\Omega_0)$ such that $u_1 = \tau_{0 \rightarrow 1}(u_0)$. Therefore,

$$\begin{aligned} \|u_1 - P_{\widehat{V}_n(\Omega_1)} u_1\| &= \|\tau_{0 \rightarrow 1}(u_0) - P_{\widehat{V}_n(\Omega_1)}(\tau_{0 \rightarrow 1}(u_0))\| \\ &\leq \|\tau_{0 \rightarrow 1}(u_0) - \tau_{0 \rightarrow 1}(P_{V_n(\Omega_0)} u_0) - P_{\widehat{V}_n(\Omega_1)}[\tau_{0 \rightarrow 1}(u_0) - \tau_{0 \rightarrow 1}(P_{V_n(\Omega_0)} u_0)]\| \\ &\quad + \|\tau_{0 \rightarrow 1}(P_{V_n(\Omega_0)} u_0) - P_{\widehat{V}_n(\Omega_1)}(\tau_{0 \rightarrow 1}(P_{V_n(\Omega_0)} u_0))\|, \end{aligned}$$

where we have added and subtracted $\tau_{0 \rightarrow 1}(P_{V_n(\Omega_0)} u_0) + P_{\widehat{V}_n(\Omega_1)}(\tau_{0 \rightarrow 1}(P_{V_n(\Omega_0)} u_0))$, and applied the triangle inequality. By applying hypothesis (H3) and (H1), we can further bound the above inequality as

$$\begin{aligned} \|u_1 - P_{\widehat{V}_n(\Omega_1)} u_1\| &\leq \|\tau_{0 \rightarrow 1}(u_0) - \tau_{0 \rightarrow 1}(P_{V_n(\Omega_0)} u_0)\| + \max_{v \in \tau_{0 \rightarrow 1} P_{V_n(\Omega_0)} \mathcal{M}(\Omega_0)} \|v - P_{\widehat{V}_n(\Omega_1)} v\| \\ &\leq C\varepsilon_0^\alpha + \max_{v \in \tau_{0 \rightarrow 1} P_{V_n(\Omega_0)} \mathcal{M}(\Omega_0)} \|v - P_{\widehat{V}_n(\Omega_1)} v\|, \end{aligned} \quad (4.8)$$

which yields inequality (4.3). Inequality (4.4) follows from using (H3) to bound $\max_{v \in \tau_{0 \rightarrow 1} P_{V_n(\Omega_0)} \mathcal{M}(\Omega_0)} \|v - P_{\widehat{V}_n(\Omega_1)} v\|$ in (4.8). Note that both inequalities (4.3) and (4.4) are suboptimal due to the construction of the bounds. \square

Theorem 4.1 shows that several ingredients are required in order to obtain a good quality reconstruction in Ω_1 from a template geometry Ω_0 :

- The quality of the reduced basis $V_n(\Omega_0)$ in Ω_0 must be high so that ε_0 is small enough.
- The transported manifold $\tau_{0 \rightarrow 1} \mathcal{M}(\Omega_0)$ must be close the target manifold $\mathcal{M}(\Omega_1)$ in the sense that η is small enough.
- The transported space $\widehat{V}_n(\Omega_1) = \widehat{\tau}_{0 \rightarrow 1}(V_n(\Omega_0))$ must have ‘‘a good alignment’’ with the observation space W in the sense that the stability constant $\beta(\widehat{V}_n(\Omega_1), W)$ is bounded away from 0.
- Finally, the transport of the space $V_n(\Omega_0)$ with $\widehat{\tau}_{0 \rightarrow 1}$ must approximate as well as possible the one with $\tau_{0 \rightarrow 1}$ so that γ is small.

4.2 An alternative error bound based on subspace distances

The reconstruction error bound (4.2) given in Theorem 4.1 involves very natural quantities such as the Hausdorff distance between the target manifold $\mathcal{M}(\Omega_1)$ and the transported one $\tau_{0 \rightarrow 1} \mathcal{M}(\Omega_0)$. The bound (4.2) may however be pessimistic in the sense that if $d_H(\tau_{0 \rightarrow 1} \mathcal{M}(\Omega_0), \mathcal{M}(\Omega_1))$ is large, then the bound will not guarantee a high quality (because η is large). In this scenario, the reconstruction may however still be of decent quality if the transported subspace $\widehat{\tau}_{0 \rightarrow 1}(V_n(\Omega_0))$ does not deviate much compared to good quality reduced subspaces $V_n(\Omega_1)$ that one could compute in the target manifold $\mathcal{M}(\Omega_1)$.

Theorem 4.2 quantifies this argument. It is a perturbative result that expresses to what extent the reconstruction is degraded between working directly with a reduced model $V_n(\Omega_1)$ and a transported subspace $\widehat{V}_n(\Omega_1) = \widehat{\tau}_{0 \rightarrow 1}(V_n(\Omega_0))$. The result involves the Hausdorff distance between the unit spheres of these two spaces, which we denote by $\mathbb{S}(V_n(\Omega_1))$ and $\mathbb{S}(\widehat{V}_n(\Omega_1))$. The square of this distance can be written as

$$\begin{aligned} d_H^2(\mathbb{S}(\widehat{V}_n(\Omega_1)), \mathbb{S}(V_n(\Omega_1))) &= \max \left(\max_{\hat{v} \in \widehat{V}_n(\Omega_1)} \frac{\|\hat{v} - P_{V_n(\Omega_1)} \hat{v}\|^2}{\|\hat{v}\|^2}; \max_{v \in V_n(\Omega_1)} \frac{\|v - P_{\widehat{V}_n(\Omega_1)} v\|^2}{\|v\|^2} \right) \\ &= \max \left(1 - \beta^2(\widehat{V}_n, V_n); 1 - \beta^2(V_n, \widehat{V}_n) \right) \\ &= 1 - \min \left(\beta^2(\widehat{V}_n, V_n); \beta^2(V_n, \widehat{V}_n) \right) \end{aligned}$$

Theorem 4.2. Let $V_n(\Omega_1)$ be a reduced model such that

$$\max_{u \in \mathcal{M}(\Omega_1)} \|u - P_{V_n(\Omega_1)} u\| \leq \varepsilon, \quad (4.9)$$

$$\beta(V_n(\Omega_1), W) \geq \underline{\beta} > 0. \quad (4.10)$$

Let $\widehat{V}_n(\Omega_1) = \widehat{\tau}_{0 \rightarrow 1}(V(\Omega_0))$ be a transported subspace from Ω_0 to Ω_1 such that

$$d_H(\mathbb{S}(\widehat{V}_n(\Omega_1)), \mathbb{S}(V_n(\Omega_1))) \leq \delta_H. \quad (4.11)$$

Then the reconstruction of $\mathcal{M}(\Omega_1)$ with PBDW using $V_n(\Omega_1)$ is well-posed and the error is bounded by

$$\max_{u \in \mathcal{M}(\Omega_1)} \|u - A_{V_n(\Omega_1)}(P_W u)\| \leq \frac{\varepsilon}{\underline{\beta}}.$$

If we use $\widehat{V}_n(\Omega_1)$, the reconstruction is well posed if and only if

$$\delta_H < \underline{\beta} \quad (4.12)$$

and the reconstruction error is bounded by

$$\max_{u \in \mathcal{M}(\Omega_1)} \|u - A_{\widehat{V}_n(\Omega_1)}(P_W u)\| \leq \frac{\varepsilon + 2\delta_H \max_{u \in \mathcal{M}(\Omega_1)} \|P_{V_n + \widehat{V}_n} u\|}{\underline{\beta}(1 - \delta_H/\underline{\beta})^{1/2}((2 + \delta_H)/\underline{\beta} - 1)^{1/2}}. \quad (4.13)$$

Proof. Let $u \in \mathcal{M}(\Omega_1)$. By direct application of (4.1), we have

$$\|u - A_{\widehat{V}_n(\Omega_1)}(P_W u)\| \leq \frac{1}{\beta(\widehat{V}_n(\Omega_1), W)} \|u - P_{\widehat{V}_n(\Omega_1)} u\|.$$

By the triangle inequality and hypothesis (4.9) and (4.11),

$$\|u - P_{\widehat{V}_n(\Omega_1)} u\| \leq \|u - P_{V_n(\Omega_1)} u\| + \|P_{V_n(\Omega_1)} u - P_{\widehat{V}_n(\Omega_1)} u\| \leq \varepsilon + 2\delta_H \|P_{V_n + \widehat{V}_n} u\|. \quad (4.14)$$

We next prove that

$$\beta^2(\widehat{V}_n, W) \geq 1 - (1 - \underline{\beta} + \delta_H)^2 = \underline{\beta}^2(1 - \delta_H/\underline{\beta})((2 + \delta_H)/\underline{\beta} - 1). \quad (4.15)$$

Note that this automatically guarantees that the reconstruction using $\widehat{V}_n(\Omega_1)$ is well-posed since, by hypothesis (4.12), we have $\delta_H < \underline{\beta}$ and therefore $\beta(\widehat{V}_n, W) > 0$.

To prove (4.15), we start from the fact that

$$\beta^2(\widehat{V}_n, W) = 1 - \max_{\hat{v} \in \widehat{V}_n} \frac{\|\hat{v} - P_W \hat{v}\|^2}{\|\hat{v}\|^2},$$

and, by Jensen's inequality, we have that for any $\zeta > 0$

$$\frac{\|\hat{v} - P_W \hat{v}\|^2}{\|\hat{v}\|^2} \leq (1 + \zeta) \frac{\|\hat{v} - v - P_W(\hat{v} - v)\|^2}{\|\hat{v}\|^2} + (1 + \zeta^{-1}) \frac{\|v - P_W v\|^2}{\|\hat{v}\|^2}, \quad \forall v \in V_n. \quad (4.16)$$

Now, on the one hand,

$$\frac{\|\hat{v} - v - P_W(\hat{v} - v)\|^2}{\|\hat{v}\|^2} \leq \frac{\|\hat{v} - v\|^2}{\|\hat{v}\|^2}. \quad (4.17)$$

On the other hand,

$$\frac{\|v - P_W v\|^2}{\|\hat{v}\|^2} \leq \frac{\|v\|^2}{\|\hat{v}\|^2} \max_{v \in V_n} \frac{\|v - P_W v\|^2}{\|v\|^2} \leq \frac{\|v\|^2}{\|\hat{v}\|^2} (1 - \underline{\beta}^2), \quad \forall v \in V_n, \quad (4.18)$$

where we have used (4.10) to derive the last inequality. Thus inserting bounds (4.17) and (4.18) into (4.16), and setting $v = P_{V_n} \hat{v}$, we derive

$$\begin{aligned} \frac{\|\hat{v} - P_W \hat{v}\|^2}{\|\hat{v}\|^2} &\leq (1 + \zeta) \frac{\|\hat{v} - P_{V_n} \hat{v}\|^2}{\|\hat{v}\|^2} + (1 + \zeta^{-1})(1 - \underline{\beta}^2) \frac{\|P_{V_n} \hat{v}\|}{\|\hat{v}\|} \\ &\leq (1 + \zeta) \max_{\hat{v} \in \widehat{V}_n} \frac{\|\hat{v} - P_{V_n} \hat{v}\|^2}{\|\hat{v}\|^2} + (1 + \zeta^{-1})(1 - \underline{\beta}^2) \\ &\leq (1 + \zeta) \delta_H^2 + (1 + \zeta^{-1})(1 - \underline{\beta}^2), \quad \forall \hat{v} \in \widehat{V}_n, \forall \zeta > 0. \end{aligned}$$

We can maximize the left-hand side over $\hat{v} \in \widehat{V}_n$ and minimize the right-hand side over $\zeta > 0$. This yields

$$\begin{aligned} 1 - \beta^2(\widehat{V}_n, W) &= \max_{\hat{v} \in \widehat{V}_n} \frac{\|\hat{v} - P_W \hat{v}\|^2}{\|\hat{v}\|^2} \\ &\leq \min_{\zeta > 0} (1 + \zeta) \delta_H^2 + (1 + \zeta^{-1})(1 - \underline{\beta}^2) \\ &= (1 - \underline{\beta} + \delta_H)^2, \end{aligned}$$

which is the proof to inequality (4.15). We derive the final result (4.13) by inserting bounds (4.15) and (4.14) into (4.5). \square

From the error bound (4.13) from Theorem 4.2, it follows that if the transported subspace $\widehat{V}_n(\Omega_1)$ deviates from $V_n(\Omega_1)$ by a quantity of the order $\delta_H \leq \varepsilon / \max_{u \in \mathcal{M}(\Omega_1)} \|u\|$, then

$$\max_{u \in \mathcal{M}(\Omega_1)} \|u - A_{\widehat{V}_n(\Omega_1)}(P_W u)\| \leq C \frac{\varepsilon}{\underline{\beta}},$$

for a relatively moderate constant $C \geq 1$. In this scenario, the reconstruction with the transported subspace is of the same quality as the one with the reduced model $V_n(\Omega_1)$ (which we are avoiding to compute in order to speed-up the state estimation procedure).

5 Transport routine τ and the routine Best-Template

5.1 Computation of $\tau_{\Omega \rightarrow \Omega'}$ and $\widehat{\tau}_{\Omega \rightarrow \Omega'}$

We next describe a practical way of a mapping snapshots and subspaces from a given geometry Ω_0 to a target geometry Ω_1 . Our approach is based on building a one-to-one mapping between the two volumes Ω_0 and Ω_1 . It involves three steps:

1. *Surface matching*: The task is to compute a map between $\partial\Omega_0$ and $\partial\Omega_1$. For this, we use the so-called Large Deformation Diffeomorphic Metric Mapping (LDDMM, see for instance [47]) method. In practice, the output of this method is an invertible and smooth mapping $T_{(\text{LDDMM})} : \partial\Omega_0 \rightarrow \partial\Omega'_1$ between $\partial\Omega_0$ and an intermediate surface $\partial\Omega'_1$ which is close to the target surface $\partial\Omega_1$. The mapping is such that, if $\partial\Omega_0 = \partial\Omega_1$, then $T_{(\text{LDDMM})}(x) = x, \forall x \in \partial\Omega_0$. The surface misfit between $\partial\Omega'_1$ and $\partial\Omega_1$ is corrected in step 3 with an interpolation post-processing.
2. *Extrapolation of the surface map to the entire volume*: We make a harmonic extension on Ω_0 and we find a displacement field $d_0 \in H^1(\Omega_0)^d$ such that

$$\begin{aligned} \Delta d_0 &= 0, \quad \text{in } \Omega_0 \\ d_0(x) &= T_{(\text{LDDMM})}(x) - x, \quad \forall x \in \partial\Omega_0. \end{aligned} \tag{5.1}$$

Note that $d_0 = 0$ if $\Omega_0 = \Omega_1$. We define the volumetric mapping

$$\begin{aligned} T_{0 \rightarrow 1'} : \Omega_0 &\rightarrow \Omega_1' \\ x_0 &\mapsto x_1 = T_{0 \rightarrow 1'}(x_0) := x_0 + d_0(x_0). \end{aligned}$$

This map is invertible and $T_{0 \rightarrow 1'}^{-1} = T_{1' \rightarrow 0}$. We further define the functional mapping

$$\begin{aligned} \phi_{0 \rightarrow 1'} : V(\Omega_0) &\rightarrow V(\Omega_1') \\ f &\mapsto \phi_{0 \rightarrow 1'}(f)(x_1') := f \circ T_{1' \rightarrow 0}(x_1'), \quad \forall x_1' \in \Omega_1'. \end{aligned}$$

3. *Interpolation:* Since in general $\Omega_1' \neq \Omega_1$, we add an interpolation operator $\mathcal{I}_{1' \rightarrow 1} : V(\Omega_1') \mapsto V(\Omega_1)$, so that the final mapping is

$$\begin{aligned} \tau_{0 \rightarrow 1} : V(\Omega_0) &\rightarrow V(\Omega_1) \\ f &\mapsto \tau_{0 \rightarrow 1}(f) := \mathcal{I}_{1' \rightarrow 1}(\phi_{0 \rightarrow 1'}(f)) \end{aligned}$$

Note that the map $\tau_{0 \rightarrow 1}$ may not exist if the spaces $V(\Omega_0)$ and $V(\Omega_1)$ are chosen of very different nature (very different regularity) or if certain physical quantities need to be preserved. One relevant example for fluid and biomedical applications is the space of divergence free fields where $V(\Omega_0) = H(\text{div}, \Omega_0)$ and $V(\Omega_1) = H(\text{div}, \Omega_1)$. In this case, for any $f \in H(\text{div}, \Omega_0)$, we have $\tau_{0 \rightarrow 1}f \in H^1(\Omega_1)$ but the function may not be divergence free. One remedy in this case is to add a post-process with the Piola transform. We therefore update the abstract definition of $\tau_{0 \rightarrow 1}$ by adding a post-process mapping p to allow this type of scenario,

$$\begin{aligned} \tau_{0 \rightarrow 1} : V(\Omega_0) &\rightarrow V(\Omega_1) \\ f &\mapsto \tau_{0 \rightarrow 1}(f) := p \circ \mathcal{I}_{1' \rightarrow 1}(\phi_{0 \rightarrow 1'}(f)). \end{aligned} \tag{5.2}$$

In our reconstruction method, we need to transport subspaces $V_n(\Omega_0) \subseteq V(\Omega_0)$ to subspaces of $V(\Omega_1)$. Note that in general the image of $V_n(\Omega_0)$ by $\tau_{0 \rightarrow 1}$, defined as

$$\tau_{0 \rightarrow 1}(V_n(\Omega_0)) := \{\tau_{0 \rightarrow 1}(v) \in V(\Omega_1) : v \in V_n(\Omega_0)\},$$

is not a linear subspace of $V(\Omega_1)$ unless $\tau_{0 \rightarrow 1}$ is a linear map. Due to this, given that in our approach we need to map subspaces into subspaces, we choose to define the image of $V_n(\Omega_0)$ with respect to a given basis $\mathcal{B} = \text{span}\{\varphi_1, \dots, \varphi_n\}$ of $V_n(\Omega_0)$ as

$$\widehat{\tau}_{0 \rightarrow 1}(V(\Omega_0), \mathcal{B}) := \text{span}\{\tau_{0 \rightarrow 1}(\varphi_1), \dots, \tau_{0 \rightarrow 1}(\varphi_n)\}$$

Note that $\widehat{\tau}_{0 \rightarrow 1}(V(\Omega_0), \mathcal{B})$ is a subspace of $V(\Omega_1)$ of dimension lower or equal to n , and it depends on the choice of the basis \mathcal{B} .

5.2 The Best-Template routine BT

The goal of this routine is to identify for each new target geometry $\Omega \in \mathbf{G}$ which template geometry $\Omega_t \in \mathbf{G}_{\text{templates}}$ has the most appropriate reduced model $V_n(\Omega_t)$ that we have to transport to Ω .

Given a target geometry $\Omega \in \mathbf{G}$ and a template geometry $\Omega_t \in \mathbf{G}_{\text{templates}}$, the reconstruction error is bounded by (see (4.1))

$$\max_{u \in \mathcal{M}(\Omega)} \|u - A_{\widehat{\tau}_{\Omega_t \rightarrow \Omega} V_n(\Omega_t)}(P_W u)\| \leq \frac{1}{\beta(\widehat{\tau}_{\Omega_t \rightarrow \Omega} V_n(\Omega_t), W)} \delta_{\Omega_t \rightarrow \Omega}^{(\text{wc})}, \tag{5.3}$$

where

$$\delta_{\Omega_t \rightarrow \Omega}^{(\text{wc})} := \max_{u \in \mathcal{M}(\Omega)} \|u - P_{\widehat{\tau}_{\Omega_t \rightarrow \Omega} V_n(\Omega_t)} u\|, \quad \forall \Omega_t \in \mathbf{G}_{\text{templates}}.$$

Alternatively, if we study errors in the average sense,

$$\mathbb{E}(\|u - A_{\widehat{\tau}_{\Omega_t \rightarrow \Omega} V_n(\Omega_t)}(P_W u)\|^2) \leq \frac{1}{\beta^2(\widehat{\tau}_{\Omega_t \rightarrow \Omega} V_n(\Omega_t), W)} \delta_{\Omega_t \rightarrow \Omega}^2, \quad (5.4)$$

with

$$\delta_{\Omega_t \rightarrow \Omega}^{(\text{ms})} := \mathbb{E}(\|u - P_{\widehat{\tau}_{\Omega_t \rightarrow \Omega} V_n(\Omega_t)} u\|^2)^{1/2}, \quad \forall \Omega_t \in \mathbf{G}_{\text{templates}}.$$

Ideally, we would like to find the template Ω_t that minimizes the upper bound (5.3) or (5.4), that is, find

$$\Omega_t^* \in \arg \min_{\Omega_t \in \mathbf{G}_{\text{templates}}} \frac{1}{\beta(\widehat{\tau}_{\Omega_t \rightarrow \Omega} V_n(\Omega_t), W_m(\Omega))} \delta_{\Omega_t \rightarrow \Omega}^{(\star\star)},$$

where $(\star\star)$ means (wc) or (ms) depending on the desired setting to study the errors. Note that this strategy depends on the observation space $W_m(\Omega)$ that we use for the reconstruction in Ω . In practice, this entails that we need to know in advance $W_m(\Omega)$ and the target Ω for the learning phase of our approach. In general, this requirement is not realistic for most applications, especially the ones from the field of biomedicine which we are particularly targeting. The procedure would have to be restarted every time that Ω and $W_m(\Omega)$ changes, making it unfeasible in real time.

There are several possibilities to avoid involving $W_m(\Omega)$ in the criterion. The option that has delivered the best results in our numerical tests is based on bound (4.13) of Theorem 4.10. From this bound, it follows that a strategy to find the best template is to minimize over the Hausdorff distance

$$d_H(\mathbb{S}(\widehat{\tau}_{\Omega_t \rightarrow \Omega} V_n(\Omega_t)), \mathbb{S}(V_n(\Omega))) \quad (5.5)$$

between a good reduced model $V_n(\Omega)$ (coming, for example, from forward reduced modeling) and the transported subspace $\widehat{\tau}_{\Omega_t \rightarrow \Omega} V_n(\Omega_t)$. With this strategy, the output to select the best-template routine is thus

$$\text{BT}(\Omega) \in \arg \min_{\Omega_t \in \mathbf{G}_{\text{templates}}} d_H(\mathbb{S}(\widehat{\tau}_{\Omega_t \rightarrow \Omega} V_n(\Omega_t)), \mathbb{S}(V_n(\Omega))). \quad (5.6)$$

In order to perform this selection in real time, we need to estimate quickly the map

$$\Omega \in \mathbf{G} \rightarrow \{d_H(\mathbb{S}(\widehat{\tau}_{\Omega_t \rightarrow \Omega} V_n(\Omega_t)), \mathbb{S}(V_n(\Omega))) : \Omega_t \in \mathbf{G}_{\text{templates}}\}.$$

In our work, this is performed with a Multidimensional Scaling approach (MDS, see e.g. [48, 49, 50, 51]). We next describe the main steps.

Remark 5.1. *Note that another criterion that does not involve $W_m(\Omega)$ is to work with $\delta_{\Omega_t \rightarrow \Omega}^{(\star\star)}$. This strategy was studied in our numerical tests but it was outperformed by the criterion (5.5) discussed in the main text. We conjecture that the reason for this is related to the fact that $\delta_{\Omega_t \rightarrow \Omega}^{(\star\star)}$ is connected to the approximation quality of the forward reduced modeling problem instead of our current inverse reconstruction problem.*

Step 1: Voxelize geometries: To ease the manipulation and comparison between different domains, we work with voxelized descriptions of them involving a uniform grid mesh of N_{vox} cells. Therefore, instead of working with a given domain $\Omega \subset \mathbb{R}^d$ with possibly involved geometry, we will actually manipulate vectors $v_\Omega \in \mathbb{R}^{N_{\text{vox}}}$ such that for all $i = 1, \dots, N_{\text{vox}}$, the voxel entry $v_\Omega^{(i)}$ is equal to the volume portion of the associated cell i of the mesh. Ideally, the size of the grid mesh N_{vox} should be large enough in order to guarantee an isomorphism between the domains $\Omega \in \mathbf{G}$ and their corresponding voxelizations v_Ω .

The family of geometries \mathbf{G} is therefore replaced in practice by the voxelized representation,

$$\mathbf{G} \sim \mathbf{V} := \{v_\Omega \in \mathbb{R}^{N_{\text{vox}}} : \Omega \in \mathbf{G}\}.$$

Similarly,

$$\mathbf{G}_{\text{templates}} \sim \mathbf{V}_{\text{templates}} := \{v_\Omega \in \mathbb{R}^{N_{\text{vox}}} : \Omega \in \mathbf{G}_{\text{templates}}\}.$$

As a result of the voxelization, we will alternatively write the manifold set of solutions $\mathcal{M}(\Omega)$ as $\mathcal{M}(v_\Omega)$ for all $\Omega \in \mathbf{G}$. Also, in practice we will construct a best template mapping of the form

$$\mathbf{BT} : \mathbb{R}^{N_v} \in \mathbf{V} \rightarrow \mathbf{V}_{\text{templates}}.$$

Learning Phase – Step 1: MDS: We consider the manifold set

$$\mathcal{S} := \{\mathcal{M}(v_\Omega) : v_\Omega \in \mathbf{V}\}.$$

Our goal is to find a low dimensional representation of \mathcal{S} using our database of K templates,

$$\mathcal{S}_{\text{templates}} := \{\mathcal{M}(v_\Omega) : v_\Omega \in \mathbf{V}_{\text{templates}}\}.$$

For this, suppose that \mathcal{S} is equipped with a metric ρ . The exact choice for ρ will be specified later on. We then assemble the matrix of pairwise square distances between elements of $\mathcal{S}_{\text{templates}}$,

$$\mathbf{D} = (d_{i,j})_{1 \leq i,j \leq K}, \quad d_{i,j} = \rho^2(\mathcal{M}(v_{\Omega_i}), \mathcal{M}(v_{\Omega_j})). \quad (5.7)$$

The vanilla version of MDS seeks to find vectors x_1, \dots, x_K from an Euclidean space \mathbb{R}^p of small dimension p such that

$$\|x_i - x_j\|_{\ell^2(\mathbb{R}^p)}^2 = d_{i,j}, \quad 1 \leq i, j \leq K.$$

The solution to this problem, if it exists, is not unique because if $\mathbf{X}^* = (x_1^* | \dots | x_K^*) \in \mathbb{R}^{p \times K}$ is a solution, then $\mathbf{X}_c^* = (x_1^* + c | \dots | x_K^* + c)$ is also a solution for any vector $c \in \mathbb{R}^p$. We therefore add a constraint in which we search for the unique centered solution such that $\sum_{i=1}^p x_{i,j}^* = 0$ for all $j = 1, \dots, K$. One can easily prove that, if such a centered solution \mathbf{X}^* exists, then it satisfies the equation

$$(\mathbf{X}^*)^T \mathbf{X}^* = \mathbf{C}, \quad (5.8)$$

with

$$\mathbf{C} := -\frac{1}{2} \mathbf{H} \mathbf{D} \mathbf{H}, \quad \mathbf{H} := \mathbf{I} - \frac{1}{K} e e^T, \quad e := \underbrace{(1, \dots, 1)}_K^T.$$

The matrix \mathbf{C} resembles a covariance matrix in that if the original pairwise distances represent Euclidean distances in a p -dimensional space, \mathbf{C} will be symmetric and positive semidefinite of rank p . Since \mathbf{C} is symmetric, its eigenvalue decomposition is of the form

$$\mathbf{C} = \mathbf{V} \mathbf{\Lambda} \mathbf{V}^T,$$

where $\mathbf{V} = (v_1 | \dots | v_K) \in \mathbb{R}^{K \times K}$ is a unitary matrix and $\mathbf{\Lambda} = \text{diag}(\lambda_1, \dots, \lambda_K)$ is a diagonal matrix containing the eigenvalues in the diagonal. We sort them in decreasing order $\lambda_1 \geq \dots \geq \lambda_K$.

If \mathbf{C} is positive definite of rank p , we have $\lambda_1 \geq \dots \geq \lambda_p > 0$ and $\lambda_i = 0$ for $p < i \leq K$. In this case, we can exactly represent the objects as points in a p -dimensional space, in such a way that the square of the Euclidean distance $\|x_i - x_j\|_{\ell^2(\mathbb{R}^p)}^2$ between each pair of points is exactly equal to $d_{i,j} = \rho^2(\mathcal{M}(v_{\Omega_i}), \mathcal{M}(v_{\Omega_j}))$. To find the points, we consider the eigenvectors v_1, \dots, v_p associated to the nonnegative eigenvalues and assemble the matrices

$$\mathbf{V}_p = (v_1 | \dots | v_p) \in \mathbb{R}^{K \times p}, \quad \mathbf{\Lambda}_p = \dots \in \mathbb{R}^{K \times p}.$$

We then set

$$\mathbf{X} = \mathbf{\Lambda}_r^{1/2} \mathbf{V}_r^T$$

Of course, in general \mathbf{C} need not be positive semi-definite, which will not be true if there is no p -dimensional embedding representing the K objects with specified pair-wise distances $d_{i,j}$. In such cases, the standard MDS procedure is to embed the data using only the positive eigenvalues. This yields an approximate embedding, whose quality depends on the importance of the eigenmodes that are discarded.

The selection of the metric for the manifold \mathcal{S} plays a critical role in the ability of MDS to find a low dimensional representation of \mathcal{S} . Ideally we would like to use $d_H^2(\mathbb{S}(\widehat{\tau}_{\Omega' \rightarrow \Omega} V_n(\Omega')), \mathbb{S}(V_n(\Omega)))$ as defined in (5.5) but the main obstacle is that this quantity is not symmetric. This is the reason why we use the symetrized version

$$\rho^2(\mathcal{M}(v_\Omega), \mathcal{M}(v_{\Omega'})) := \frac{1}{2} d_H^2(\mathbb{S}(\widehat{\tau}_{\Omega' \rightarrow \Omega} V_n(\Omega')), \mathbb{S}(V_n(\Omega))) + \frac{1}{2} d_H^2(\mathbb{S}(V_n(\Omega')), \mathbb{S}(\widehat{\tau}_{\Omega \rightarrow \Omega'} V_n(\Omega))) \quad (5.9)$$

Note that the above mapping $\rho : \mathcal{S} \times \mathcal{S} \mapsto \mathbb{R}_+$ does not define a distance in the classical sense because it does not satisfy the triangle inequality. Despite this, the fact that it is symmetric is sufficient to perform the MDS procedure. We will see that this choice yields good results despite the fact that we do not work with a metric. The success of our choice may be connected to the fact that our function ρ involves a notion of ordering since we have that $0 = \rho(\mathcal{M}(v_\Omega), \mathcal{M}(v_\Omega)) < \rho(\mathcal{M}(v_\Omega), \mathcal{M}(v_{\Omega'}))$ if $\Omega' \neq \Omega$.

Learning Phase – Step 2: Voxelization-to-embedding-space Mapping: The final element in our procedure is to build a mapping between the voxelization v_Ω of a geometry $\Omega \in \mathbf{G}$ and the corresponding point $x_\Omega \in \mathbb{R}^p$ in the low dimensional parametrization of \mathcal{S} . In our case, this step is done by a simple linear least-squares procedure but of course other options could be considered. We search for a minimizer of

$$\min_{\mathbf{W} \in \mathbb{R}^{N_{\text{vox}} \times p}} \frac{1}{2K} \sum_{\Omega \in \mathbf{G}_{\text{templates}}} \|\mathbf{W}^T v_\Omega - x_\Omega\|_{\ell^2(\mathbb{R}^p)}^2.$$

Denoting $\mathbf{V} = (v_{\Omega_1} | \dots | v_{\Omega_K}) \in \mathbb{R}^{N_{\text{vox}} \times K}$ and $\mathbf{X} = (x_{\Omega_1} | \dots | x_{\Omega_K}) \in \mathbb{R}^{p \times K}$, the solution \mathbf{W} with minimal norm satisfies the least-squares equation

$$\mathbf{V}\mathbf{V}^T \mathbf{W} = \mathbf{V}\mathbf{X},$$

which can be solved by classical least-squares inversion techniques.

Practical Application of the routine BT: Once the above learning steps have been performed, given a domain $\Omega \in \mathbf{G}$ we can quickly find the best template from $\mathbf{G}_{\text{templates}}$ by performing the following steps:

- Compute the corresponding voxelization v_Ω of the target geometry Ω .
- Find the representation of $\mathcal{M}(v_\Omega)$ in the low-dimensional space by computing $x_\Omega = \mathbf{W}^T v_\Omega$.
- Find the template geometry which is the closest in the embedding

$$\Omega_t^* \in \arg \min_{\Omega_t \in \mathbf{G}_{\text{templates}}} \|x_\Omega - x_{\Omega_t}\|_{\ell^2(\mathbb{R}^p)}^2 \quad (5.10)$$

and set $\text{BT}(\Omega) = \Omega_t^*$. This choice is justified from the following fact: our original minimization problem is (5.6), that is, to find

$$\min_{\Omega_t \in \mathbf{G}_{\text{templates}}} d_H(\mathbb{S}(\widehat{\tau}_{\Omega_t \rightarrow \Omega} V_n(\Omega_t)), \mathbb{S}(V_n(\Omega))).$$

By definition (5.9) of the metric ρ ,

$$d_H(\mathbb{S}(\widehat{\tau}_{\Omega_t \rightarrow \Omega} V_n(\Omega_t)), \mathbb{S}(V_n(\Omega))) \leq \sqrt{2} \rho(\mathcal{M}(v_\Omega), \mathcal{M}(v_{\Omega_t})) \approx \sqrt{2} \|x_\Omega - x_{\Omega_t}\|_{\ell^2(\mathbb{R}^p)}$$

Therefore, our choice (5.10) for Ω_t^* guarantees that

$$\min_{\Omega_t \in \mathbf{G}_{\text{templates}}} d_H(\mathbb{S}(\widehat{\tau}_{\Omega_t \rightarrow \Omega} V_n(\Omega_t)), \mathbb{S}(V_n(\Omega))) \lesssim \sqrt{2} \|x_\Omega - x_{\Omega_t^*}\|_{\ell^2(\mathbb{R}^p)}.$$

6 Numerical example

The proposed methodology is general and, among the many different applications that could be envisaged, problems from the field of biomedicine emerge as particularly relevant. As such, we next present a numerical example on this topic related to the task of reconstructing 3D blood velocity flows from Doppler ultrasound velocity images (see [41, 46]). The tests are performed on synthetically generated observations due to our lack of real data. The linear observation functions $\{\ell_i\}_{i=1}^m$ will thus be defined in order to mimic the output of real ultrasound images.

Sections 6.1 to 6.3 give details on the test case, and outline the steps performed for the training phase. The training follows exactly the guidelines given in section 3. Section 6.4 quantifies and illustrates the good performance of the reconstruction strategy.

6.1 Geometry

In our example, the family G of geometries is a set of 3D Venturi tubes with variations on three geometrical parameters concerning the tube coarctation (see Figure 1). The parameters are the coarctation length S_l , its radius S_r , and its position along the y -axis S_x . The ranges of the geometrical parameters are $S_r \in [1.4, 2.6]$ mm, $S_l \in [0.8L, 1.2L]$ and $S_x \in [5, 11]$ mm. The length of the tube is fixed to $L = 5$ cm, and its diameter to $D = 0.4$ cm.

Training Phase: We work with $K = 64$ template geometries for the database $G_{\text{templates}}$. They are computed using a uniform grid sample on the three geometrical parameters.

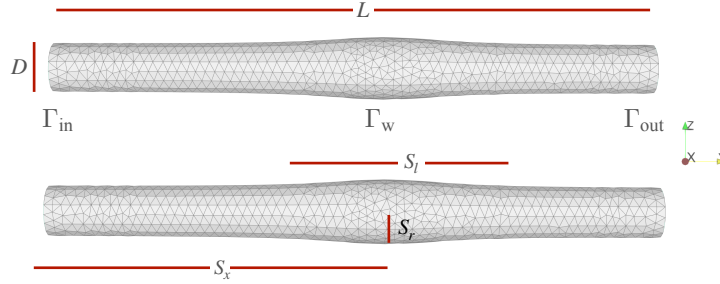


Figure 1: Scheme for the generation of the set G .

6.2 Physics, solution manifold $\mathcal{M}(\Omega)$, and reduced model $V_n(\Omega)$

We assume that the fluid is governed by the Stokes equations defined, for a given $\Omega \in G$, as the problem of finding the velocity $u \in [H^1(\Omega; [0, T])]^3$ and the pressure $p \in L^2(\Omega; [0, T])$ such that:

$$\left\{ \begin{array}{l} \partial_t u - \mu \Delta u + \nabla p = 0 \text{ in } \Omega \\ \nabla \cdot u = 0 \text{ in } \Omega \\ u = (0, 0, 0) \text{ on } \Gamma_w \\ u = u_0 \left(0, 1 - \frac{x^2 + z^2}{(D/2)^2}, 0 \right) \sin(2\pi t) \text{ on } \Gamma_{\text{in}} \\ \left(\frac{\nabla^T u + \nabla u}{2} - p \mathbf{I} \right) \cdot n = (0, 0, 0) \text{ on } \Gamma_{\text{out}} \end{array} \right. \quad (6.1)$$

where \mathbf{I} is an identity matrix of size three, n is a unitary vector pointing outwards the working domain, and $u_0 \in \mathbb{R}_+$. The boundary $\partial\Omega$ is decomposed into 3 disjoint subdomains,

$$\partial\Omega = \Gamma_{\text{in}} \cup \Gamma_{\text{out}} \cup \Gamma_{\text{w}},$$

where Γ_{in} is the inflow part, Γ_{out} the outflow, and Γ_{w} corresponds to the walls (see Figure 1).

In our example, we reconstruct velocities taking $V(\Omega) = [L^2(\Omega)]^3$ as the ambient reconstruction space. Note that this does not match with the space $[H^1(\Omega)]^3$ in which velocity is defined in the Stokes equation. This choice was made in order to target the reconstruction of the field and not its derivatives.

For each $\Omega \in \mathcal{G}$, we work with the manifold

$$\mathcal{M}(\Omega) := \{u(y) : y \in Y\},$$

with

$$Y := \{y = (t, u_0, \mu) \in [0, 0.5 \text{ s.}] \times [0.01, 1 \text{ cm/s}] \times [0.01, 0.1 \text{ P}]\}.$$

Training Phase: For each $\Omega \in \mathcal{G}_{\text{templates}}$, we compute a finite training subset of $\mathcal{M}(\Omega)$ with $N_s = 12\,800$ snapshots, and we compute its Proper Orthogonal Decomposition (POD). The parameters to generate the snapshots are sampled from a uniform random distribution. Appendix A gives some details on the discretization and the solver used to generate them. The reduced order model $V_n(\Omega)$ is the subspace spanned by the POD eigenfunctions associated to the $n = 20$ most energetic modes.

6.2.1 Example of $\hat{\tau}_{0 \rightarrow 1}$ for mass conservative fields

We have described in section 5.1 how fields are transported among domains. Let us illustrate the methodology with a numerical example between two geometries Ω_0 and Ω_1 , as shown in figure 2.a and 2.b, respectively. Let $v_{st} \in [H^1(\Omega)]^3$ be a divergence free vector field, depicted on figure 2.a and solution to the Stokes problem (6.1), a snapshot in the training set of Ω_0 . In figure 2.b we observe the result of the shape registration via LDDMM (implemented using [52]) computed from (5.1). Mass conservation is not preserved nonetheless. In order to convey a divergence free field in the arrival geometry we define the operator p from equation (5.2) as the Piola transform $p : [H^1(\Omega_0)]^3 \mapsto [H^1(\Omega_1)]^3$ (see [53] or [32]):

$$p(v) = \frac{(I_{3 \times 3} + \nabla [\mathcal{I}_{1 \rightarrow 1'} \circ \phi_{0 \rightarrow 1'}(d_0)])}{\det(I_{3 \times 3} + \nabla [\mathcal{I}_{1' \rightarrow 1} \circ \phi_{0 \rightarrow 1'}(d_0)])} \mathcal{I}_{1' \rightarrow 1} \circ \phi_{0 \rightarrow 1'}(v).$$

In figure 2.c we observe how this transformation recovers mass conservation in Ω_1 . The underlying mechanism of this operator is well illustrated with the scaling factor of figure 2.d.

6.3 MDS

We compute the MDS from the spectrum of the inner product matrix (5.8). To do so, we first compute the matrix $\mathbf{D} = (d_{i,j})_{1 \leq i,j \leq K}$ of pairwise distances between the $K = 64$ templates (see (5.7)). Each entry $d_{i,j}$ is computed using formula (5.9) to quantify distances between two manifolds on different geometries.

To visually illustrate the methodology, we select a subset of $\tilde{K} = 16$ and show in Figure 3(a) the values $d_{i,j}$ of the matrix \mathbf{D} . Figure 3(b) shows the positions x_Ω in the reduced Euclidean space of dimension $p = 2$ for the \tilde{K} geometries. It is interesting to remark that the low dimensional representation of the geometries reflects the main differences in the geometrical parameters despite that the MDS methodology is fully non-parametric. The figure shows that the “dominant” parameter that drives metric changes is the radius S_r since the points x_Ω tend to cluster following its values. For $\tilde{K} = 16$ geometries a bi-dimensional representation is enough to get a good embedding. For $K = 64$ geometries, we work in \mathbb{R}^3 .

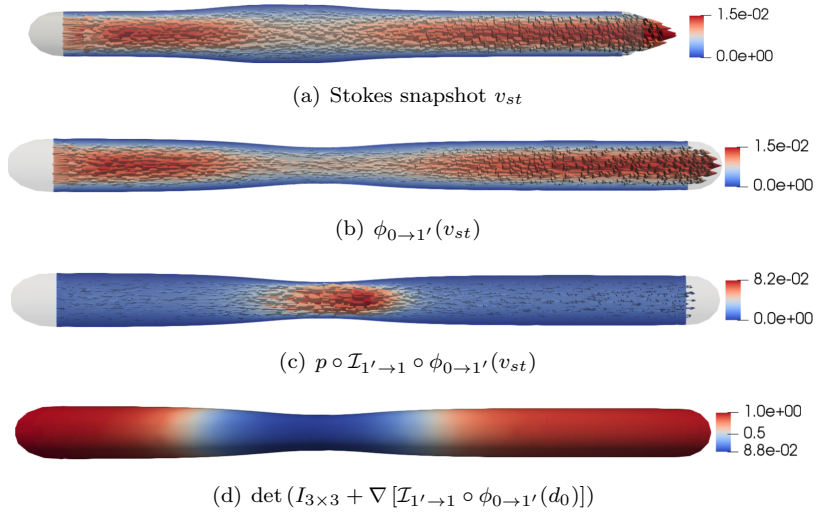


Figure 2: A divergence free field transported among geometries with a different value for S_r .

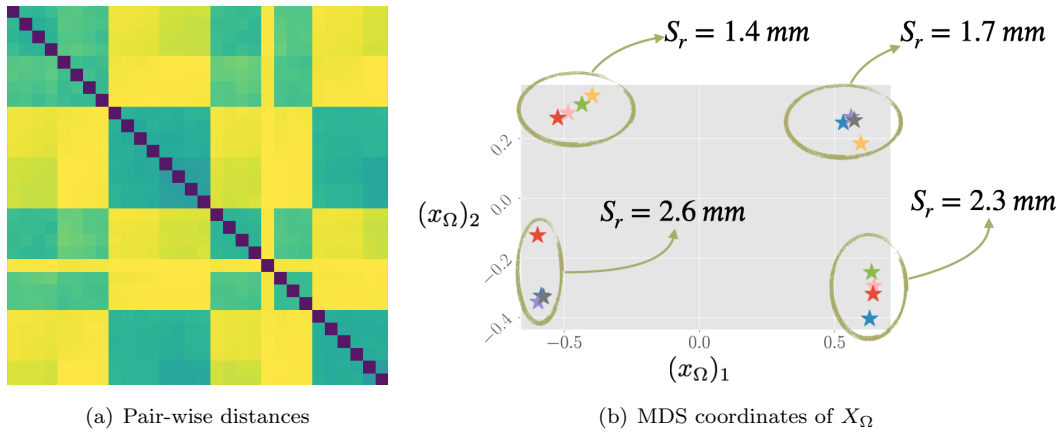


Figure 3: Pair-wise distances plot (normalized scale in $[0,1]$, where blue is 0 and yellow is 1) between 16 geometries and MDS representation in \mathbb{R}^2 .

6.4 Reconstruction of synthetic data

Definition of the observation space $W_m(\Omega)$: For a given $\Omega \in \mathcal{G}$, we consider a partition of $\Omega = \cup_{i=1}^m \Omega_i^{\text{voxel}}$ into m disjoint subdomains (voxels) Ω_i^{voxel} . We mimic getting ultrasound images by defining the linear functionals $\ell_i \in L^2(\Omega)$ as

$$\ell_i(u) = \int_{\Omega_i^{\text{voxel}}} u \cdot b \, dx, \quad 1 \leq i \leq m,$$

where b is a unitary vector giving the direction of the ultrasound beam. In our case, the plane is chosen to be $z = 0$, the ultrasound direction is $b = [0, \sqrt{2}/2, \sqrt{2}/2]$ and the size of voxels is 2.5 mm^3 . The dimension m of the total number of observations changes slightly between geometries. The geometry with the smallest amount of voxels, i.e., the geometry corresponding to the smaller parameter S_r and maximal S_l , is $m = 59$. Given that the domain is unknown a-priori, we need to address the construction of the space $W_m(\Omega) = \text{span}\{\omega_i\}_{i=1}^m$ during the online phase. The problem of computing the Riesz representers of the measures reads: Find $\{\omega_i\}_{i=1}^m \in V$ such that

$$\langle \omega_i, v \rangle_{V(\Omega)} = \int_{\Omega_i^{\text{voxel}}} v \cdot b \, dx \quad \forall v \in V(\Omega),$$

Since our reconstruction space $V(\Omega)$ is $L^2(\Omega)$, we have that $\omega_i = \mathbb{1}_{\Omega_i^{\text{voxel}}} b$, and the numerical cost of computing the family of representers $\{\omega_i\}_{i=1}^m$ is negligible in our case. In Figure 4 we give an example of a PDE solution u and its associated synthetic Doppler ultra-sound data $P_{W_m} u$.

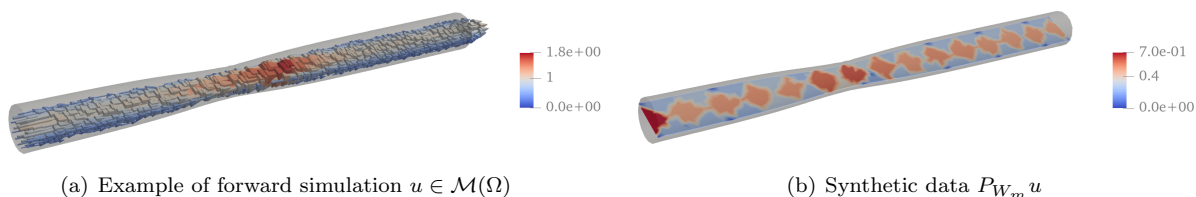


Figure 4: Snapshot in manifold of solutions and its projection in the space W_m . The measures emulates Doppler ultrasound data with a transducer steered with an angle of $\pi/4$ respect to the main fluid direction.

Reconstruction: We test the methodology with $K_{\text{test}} = 16$ test working domains $G_{\text{test}} = \{\Omega_i^{\text{test}}\}_{i=1}^{K_{\text{test}}}$ which are taken different from the geometries in $G_{\text{templates}}$. For each test working domain, we sample $N_{\text{target}} = 16$ target simulations of the governing dynamics in $\mathcal{M}(\Omega_t^i)$. This yields a total of 50 snapshots per target due to time marching.

We study the performance of our method in terms of relative average reconstruction errors in L^2 . For a given target geometry $\Omega \in G_{\text{test}}$, if we reconstruct by transporting reduced model $V_n(\Omega_t)$ from a given template geometry $\Omega_t \in G_{\text{templates}}$, the relative error for the i -th simulation at time t is defined as

$$e_{\Omega_t \rightarrow \Omega}^i(t) = \frac{\|u_i(t) - A(P_{W_m} u(t))\|}{\left(\int_0^T \|u_i(t)\|^2 dt\right)^{1/2}}. \quad (6.2)$$

In Figure 5, we fix one target geometry $\Omega \in G_{\text{test}}$ and we show the average error over all simulations i , namely

$$e_{\Omega_t \rightarrow \Omega}(t) = \frac{1}{N_{\text{target}}} \sum_{i=1}^{N_{\text{target}}} e_{\Omega_t \rightarrow \Omega}^i(t).$$

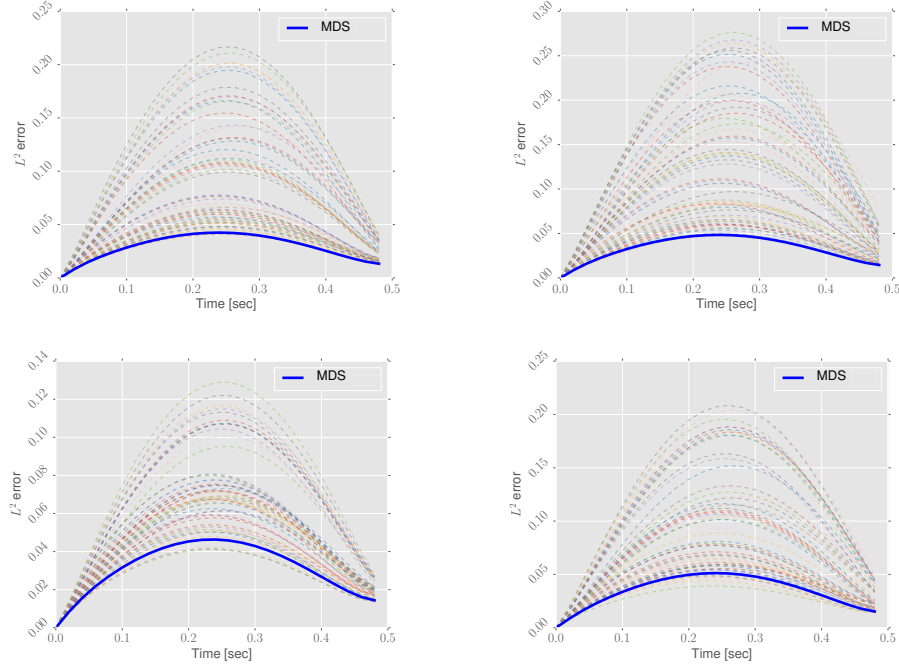


Figure 5: The reconstruction error (6.2) with the best template for 4 different target geometries $\Omega \in G_{\text{test}}$. The **Best-Template** method is able to identify a good or the best template.

Each curve depicts the error for each template geometry $\Omega_t \in G_{\text{templates}}$. The role of the routine **Best-Template** which we have built in the learning stage is to quickly select the template which will be the most appropriate so that we obtain the most accurate reconstruction results. The selection with our proposed construction yields the error curve which is labeled MDS. We tested several possibilities for the definition of the metric ρ but the one based (5.9) produced systematically the best results, so, for the sake of clarity, we only present the results for this choice. We observe in Figure 5 that the selection method is near-optimal in the sense that it chooses either a good or the best available template among the 64 template domains. Figure 6 gives an illustration of the reconstruction of one snapshot with our pipeline.

In addition, it is important to compare with a set of reconstructions on all the K_{test} test geometries $\Omega_{\text{test}} \in G_{\text{test}}$ with the pre-computed ROMs $V_n(\Omega_{\text{test}})$. We want to quantify the difference between the PBDW algorithm output of $A_{V_n(\Omega_{\text{test}})}(\omega)$ and that of $A_{\hat{V}_n(\Omega)}(\omega)$, for $\omega \in W_m$. We recall that $\hat{V}_n(\Omega) = \hat{\tau}_{\Omega_t^* \rightarrow \Omega}(V_n(\Omega_t^*))$, and $\Omega_t^* = \text{BT}(\Omega_{\text{test}})$.

It is encouraging to observe that the relative error

$$\max_i \frac{\|A_{V_n(\Omega_{\text{test}})}(\omega_i) - A_{\hat{V}_n(\Omega)}(\omega_i)\|_{L^2}}{\|u_{\text{GT}}^i\|_{L^2}}$$

is below one percent for a set of 16 ground truth solutions $\{u_{\text{GT}}^i\}_{i=1}^{16}$ in each test domain Ω_{test} , with $\omega_i = P_{W_m}(u_{\text{GT}}^i)$.

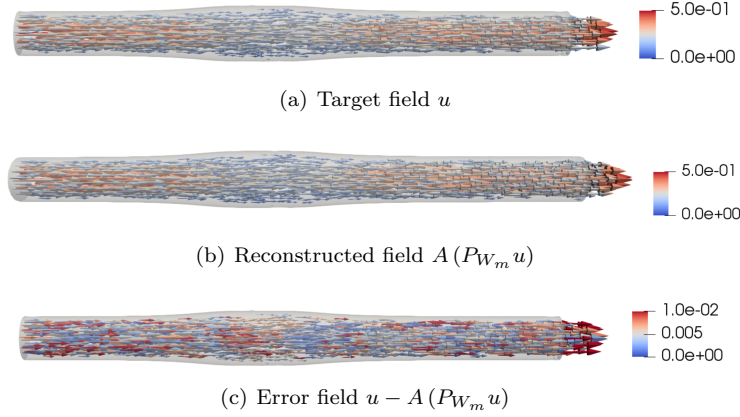


Figure 6: Example of field reconstruction for one target snapshot

7 Conclusion

We have developed a framework to solve in near-real time state estimation problems for applications that present variations in the spatial domain. For a given target geometry, the reconstruction strategy is based on selecting a relevant reduced model defined on a template geometry, which is then transported to the target geometry. The reduced model is chosen among a pool of available reduced models, each one defined on a different template geometry. The model selection strategy is based on a dimensionality reduction technique based on MDS. The technique requires defining an appropriate notion of distance between manifold sets $\mathcal{M}(\Omega)$ from different geometries Ω . Among the different options for the metric which we have tested in our numerical experiments, the one based on formula (5.9) has produced the best results, and is simple to implement in practice. This choice is backed up by our theoretical analysis from Theorem 4.2.

The present contribution paves the way for further developments in the field of inverse problems presenting shape variability, especially in the field of biomedical engineering. Future research will be devoted to applying the present methodology to applications with real data, and for which the shape of the target domain evolves in time.

Appendix

A Details on the numerical solution of the Stokes equation

Using finite elements, we search for the projection coefficients of u and p in the space of piece-wise linear polynomials $[\mathbb{P}_1(\Omega_h)]^3$ and $\mathbb{P}_1(\Omega_j)$ respectively. The Lagrange polynomials are considered on Ω_h , a tessellation of Ω with tetrahedrons of size $h = 0.08$ cms. We don't adopt a new notation for the projection of the states in the polynomial spaces when no confusion arises. Time discretization is done via implicit finite differences using a time step of $\Delta t = 0.02$ seconds. The semi-discrete weak problem to solve for each u^{n+1} reads:

$$\frac{1}{\Delta t} \langle u^{n+1}, v \rangle + \mu \langle \nabla u^{n+1}, \nabla v \rangle - \langle p, \nabla \cdot v \rangle + \langle \nabla \cdot u^{n+1}, q \rangle + \sum_{\text{Tet}} h_{\text{Tet}}^2 \langle \nabla p, \nabla q \rangle_K = \frac{1}{\Delta t} \langle u^n, v \rangle,$$

$\forall (v, q) \in [H^1(\Omega)]^3 \times L^2(\Omega)$, where v and q are test functions and where $\langle \cdot, \cdot \rangle$ denotes the inner product in $L^2(\Omega)$. In addition, $\langle \cdot, \cdot \rangle_{\text{Tet}}$ denotes the $L^2(\Omega_h)$ inner product over a single tetrahedron Tet in Ω_h .

The bilinear form concerning this term is a typical stabilization procedure to deal with the saddle point nature of the problem [54].

The matrix assemblage and solution of the monolithic system of equations is done with CPU parallelization via MPI using the software MAD ([55], chapter 5).

References

- [1] Alfio Quarteroni, Andrea Manzoni, and Federico Negri. *Reduced basis methods for partial differential equations: an introduction*, volume 92. Springer, 2015.
- [2] Peter Benner, Mario Ohlberger, Albert Cohen, and Karen Willcox. *Model reduction and approximation: theory and algorithms*. SIAM, 2017.
- [3] B. Lahoz and R. Menard. *Data assimilation*. Springer, 2010.
- [4] G. Evensen. *Data assimilation: the ensemble Kalman filter*. Springer Science & Business Media, 2009.
- [5] Michalis Frangos, Youssef Marzouk, Karen Willcox, and B van Bloemen Waanders. Surrogate and reduced-order modeling: a comparison of approaches for large-scale statistical inverse problems [chapter 7]. 2010.
- [6] Mark Kaercher, Sébastien Boyaval, Martin A Grepl, and Karen Veroy. Reduced basis approximation and a posteriori error bounds for 4d-var data assimilation. *Optimization and Engineering*, 19(3):663–695, 2018.
- [7] Benjamin Peherstorfer and Karen Willcox. Dynamic data-driven reduced-order models. *Computer Methods in Applied Mechanics and Engineering*, 291:21–41, 2015.
- [8] Stefano Pagani, Andrea Manzoni, and Alfio Quarteroni. Efficient state/parameter estimation in nonlinear unsteady pdes by a reduced basis ensemble kalman filter. *SIAM/ASA Journal on Uncertainty Quantification*, 5(1):890–921, 2017.
- [9] Răzvan Ștefănescu, Adrian Sandu, and Ionel Michael Navon. Pod/deim reduced-order strategies for efficient four dimensional variational data assimilation. *Journal of Computational Physics*, 295:569–595, 2015.
- [10] Rhodri Davies, Carole Twining, and Chris Taylor. *Statistical models of shape: Optimisation and evaluation*. Springer Science & Business Media, 2008.
- [11] Aymeric Maury, Grégoire Allaire, and François Jouve. Shape optimisation with the level set method for contact problems in linearised elasticity. *The SMAI journal of computational mathematics*, 3:249–292, 2017.
- [12] Frederic De Gournay, Grégoire Allaire, and François Jouve. Shape and topology optimization of the robust compliance via the level set method. *ESAIM: Control, Optimisation and Calculus of Variations*, 14(1):43–70, 2008.
- [13] David L Colton, Rainer Kress, and Rainer Kress. *Inverse acoustic and electromagnetic scattering theory*, volume 93. Springer, 1998.
- [14] Fred L Bookstein. *A course in morphometrics for biologists: geometry and statistics for studies of organismal form*. Cambridge University Press, 2018.
- [15] Philipp Mitteroecker and Philipp Gunz. Advances in geometric morphometrics. *Evolutionary Biology*, 36(2):235–247, 2009.

- [16] Alf Emil Løvgrén, Yvon Maday, and Einar M Rønquist. The reduced basis element method for fluid flows. In *Analysis and Simulation of Fluid Dynamics*, pages 129–154. Springer, 2006.
- [17] Gianluigi Rozza, DB Phuong Huynh, and Andrea Manzoni. Reduced basis approximation and a posteriori error estimation for stokes flows in parametrized geometries: roles of the inf-sup stability constants. *Numerische Mathematik*, 125(1):115–152, 2013.
- [18] Andrea Manzoni and Federico Negri. Efficient reduction of pdes defined on domains with variable shape. In *Model Reduction of Parametrized Systems*, pages 183–199. Springer, 2017.
- [19] Niccolò Dal Santo and Andrea Manzoni. Hyper-reduced order models for parametrized unsteady navier-stokes equations on domains with variable shape. *Advances in Computational Mathematics*, 45(5):2463–2501, 2019.
- [20] Ludovic Chamoin and HP Thai. Certified real-time shape optimization using isogeometric analysis, pgd model reduction, and a posteriori error estimation. *International Journal for Numerical Methods in Engineering*, 119(3):151–176, 2019.
- [21] Fabrizio Garotta, Nicola Demo, Marco Tezzele, Massimo Carraturo, Alessandro Reali, and Gianluigi Rozza. Reduced order isogeometric analysis approach for pdes in parametrized domains. In *Quantification of Uncertainty: Improving Efficiency and Technology*, pages 153–170. Springer, 2020.
- [22] Ruben Sevilla, Sergio Zlotnik, and Antonio Huerta. Solution of geometrically parametrised problems within a cad environment via model order reduction. *Computer methods in applied mechanics and engineering*, 358:112631, 2020.
- [23] Filippo Salmoiraghi, Angela Scardigli, Haysam Telib, and Gianluigi Rozza. Free-form deformation, mesh morphing and reduced-order methods: enablers for efficient aerodynamic shape optimisation. *International Journal of Computational Fluid Dynamics*, 32(4-5):233–247, 2018.
- [24] Efthymios N Karatzas, Giovanni Stabile, Leo Nouveau, Guglielmo Scovazzi, and Gianluigi Rozza. A reduced basis approach for pdes on parametrized geometries based on the shifted boundary finite element method and application to a stokes flow. *Computer Methods in Applied Mechanics and Engineering*, 347:568–587, 2019.
- [25] Nissrine Akkari, Fabien Casenave, and David Ryckelynck. A novel gappy reduced order method to capture non-parameterized geometrical variation in fluid dynamics problems. 2019.
- [26] Efthymios N Karatzas, Francesco Ballarin, and Gianluigi Rozza. Projection-based reduced order models for a cut finite element method in parametrized domains. *Computers & Mathematics with Applications*, 79(3):833–851, 2020.
- [27] Giovanni Stabile, Matteo Zancanaro, and Gianluigi Rozza. Efficient geometrical parametrization for finite-volume-based reduced order methods. *International Journal for Numerical Methods in Engineering*, 121(12):2655–2682, 2020.
- [28] Davide Forti and Gianluigi Rozza. Efficient geometrical parametrisation techniques of interfaces for reduced-order modelling: application to fluid–structure interaction coupling problems. *International Journal of Computational Fluid Dynamics*, 28(3-4):158–169, 2014.
- [29] Martin W Hess and Peter Benner. A reduced basis method for microwave semiconductor devices with geometric variations. *COMPEL: The International Journal for Computation and Mathematics in Electrical and Electronic Engineering*, 2014.
- [30] Tommaso Taddei. A registration method for model order reduction: data compression and geometry reduction. *SIAM Journal on Scientific Computing*, 42(2):A997–A1027, 2020.

- [31] Tommaso Taddei and Lei Zhang. Space-time registration-based model reduction of parameterized one-dimensional hyperbolic pdes. *arXiv preprint arXiv:2004.06693*, 2020.
- [32] Romain Guibert, Kristin Mcleod, Alfonso Caiazzo, Tommaso Mansi, Miguel A Fernández, Maxime Sermesant, Xavier Pennec, Irene E Vignon-Clementel, Younes Boudjemline, and Jean-Frédéric Gerbeau. Group-wise construction of reduced models for understanding and characterization of pulmonary blood flows from medical images. *Medical image analysis*, 18(1):63–82, 2014.
- [33] Y. Maday, A. T. Patera, J. D. Penn, and M. Yano. A parameterized-background data-weak approach to variational data assimilation: formulation, analysis, and application to acoustics. *International Journal for Numerical Methods in Engineering*, 102(5):933–965, 2015.
- [34] Y. Maday, O. Mula, and G. Turinici. Convergence analysis of the Generalized Empirical Interpolation Method. *SIAM Journal on Numerical Analysis*, 54(3):1713–1731, 2016.
- [35] P. Binev, A. Cohen, W. Dahmen, R. DeVore, G. Petrova, and P. Wojtaszczyk. Data assimilation in reduced modeling. *SIAM/ASA Journal on Uncertainty Quantification*, 5(1):1–29, 2017.
- [36] T. Taddei. An adaptive parametrized-background data-weak approach to variational data assimilation. *ESAIM: Mathematical Modelling and Numerical Analysis*, 51(5):1827–1858, 2017.
- [37] P. Binev, A. Cohen, O. Mula, and J. Nichols. Greedy algorithms for optimal measurements selection in state estimation using reduced models. *SIAM/ASA Journal on Uncertainty Quantification*, 6(3):1101–1126, 2018.
- [38] H. Gong, Y. Maday, O. Mula, and T. Taddei. PBDW method for state estimation: error analysis for noisy data and nonlinear formulation. *arXiv e-prints*, page arXiv:1906.00810, Jun 2019.
- [39] A. Cohen, W. Dahmen, R. DeVore, J. Fadili, O. Mula, and J. Nichols. Optimal reduced model algorithms for data-based state estimation. *SIAM Journal on Numerical Analysis*, 58(6):3355–3381, 2020.
- [40] A. Cohen, W. Dahmen, O. Mula, and J. Nichols. Nonlinear reduced models for state and parameter estimation. *arXiv:2009.02687*, 2020.
- [41] F. Galarce, J.F. Gerbeau, D. Lombardi, and O. Mula. Fast reconstruction of 3d blood flows from doppler ultrasound images and reduced models. *Computer Methods in Applied Mechanics and Engineering*, 375:113559, 2021.
- [42] A. Cohen and R. DeVore. Approximation of high-dimensional parametric pdes. *Acta Numerica*, 24:1–159, 2015.
- [43] A. Buffa, Y. Maday, A. T. Patera, C. Prud’homme, and G. Turinici. A priori convergence of the greedy algorithm for the parametrized reduced basis method. *ESAIM: Mathematical Modelling and Numerical Analysis*, 46(3):595–603, 2012.
- [44] G. Rozza, D. B. P. Huynh, and A. T. Patera. Reduced basis approximation and a posteriori error estimation for affinely parametrized elliptic coercive partial differential equations. *Archives of Computational Methods in Engineering*, 15(3):1, Sep 2007.
- [45] A. Cohen, R. DeVore, and C. Schwab. Analytic regularity and polynomial approximation of parametric and stochastic elliptic PDE’s. *Analysis and Applications*, 09(01):11–47, 2011.
- [46] F. Galarce, D. Lombardi, and O. Mula. Reconstructing haemodynamics quantities of interest from doppler ultrasound imaging. *Int. J. Numer. Meth. Biomedical Eng.*, 2021.
- [47] M. Faisal Beg, Michael I. Miller, Alain Trounev, and Laurent Younes. Computing large deformation metric mappings via geodesic flows of diffeomorphisms. *International Journal of Computer Vision*, 65:139–157, 2005.

- [48] H. Murase and S. K. Nayar. Visual learning and recognition of 3-d objects from appearance. *International journal of computer vision*, 14(1):5–24, 1995.
- [49] J. B. Tenenbaum, V. De Silva, and J. C. Langford. A global geometric framework for nonlinear dimensionality reduction. *science*, 290(5500):2319–2323, 2000.
- [50] D. L. Donoho and C. Grimes. Image manifolds which are isometric to euclidean space. *Journal of mathematical imaging and vision*, 23(1):5–24, 2005.
- [51] B. Ghojogh, A. Ghodsi, F. Kararray, and M. Crowley. Multidimensional scaling, sammon mapping, and isomap: Tutorial and survey. *arXiv preprint arXiv:2009.08136*, 2020.
- [52] Benjamin Charlier, Jean Feydy, Joan Alexis Glaunès, François-David Collin, and Ghislain Durif. Kernel operations on the gpu, with autodiff, without memory overflows. *Journal of Machine Learning Research*, 22(74):1–6, 2021.
- [53] P. Ciarlet. *Mathematical Elasticity, vol. I, Studies in Mathematics and its Applications*, volume 20. North-Holland Publishong Co., 1988.
- [54] F. Brezzi and J. Pitkaranta. On the stabilization of finite element approximations of the stokes equations. *Efficient Solutions of Elliptic Systems*, 1984.
- [55] F. Galarce Marin. *Inverse problems in hemodynamics. Fast estimation of blood flows from medical data*. PhD thesis, INRIA Paris & Laboratoire Jacques-Louis Lions. Sorbonne Université, 2021.